Lab on a Chip

PAPER

View Article Online
View Journal | View Issue

Cite this: *Lab Chip*, 2025, **25**, 4787

A high-speed sequential liquid compartmentalization method for digital loop-mediated isothermal amplification in a microfluidic device

Riku Honda,*[a] Taketo Saruwatari,[a] Daigo Natsuhara,[bc] Yuka Kiba,[d] Shunya Okamoto,[a] Moeto Nagai,[ae] Masashi Kitamura[d] and Takayuki Shibata *[ae]

Accurate and rapid quantification of nucleic acid targets is crucial for molecular diagnostics, particularly in resource-limited settings where simple and robust technologies are required. This study presents a high-throughput digital loop-mediated isothermal amplification (dLAMP) platform for the absolute quantification of nucleic acids in a sample, using a microfluidic device comprising ten thousand nanoliter-scale reaction microchambers. The polydimethylsiloxane (PDMS)-based device achieved complete liquid compartmentalization within 60 s in a single operation using an electronic pipette, without requiring surface modification, pre-degassing, pre-priming, or external pumping systems, which are typically necessary in conventional methods. The aqueous sample/reagent mixture was reliably compartmentalized using fluorinated oil, with 97% of the microchambers successfully filled to at least 80% of their designed volume, exhibiting excellent volumetric uniformity (CV = 0.07). Fluorescent LAMP assays targeting *Salmonella* and cannabis exhibited strong correlations between estimated and true DNA concentrations ($R^2 > 0.98$), although quantification was consistently underestimated. Correction factors of 1000 and 10 000 were required for synthetic *Salmonella* and cannabis DNA, respectively, whereas only 10 were needed for cannabis seed-derived DNA, indicating these discrepancies were due to the intrinsic performance of the LAMP assays rather than device limitations. The dLAMP device also enabled the successful detection of cannabis seed DNA in the presence of 10 ng μL^{-1} humic acid, which inhibits amplification in conventional turbidity-based LAMP, demonstrating its robustness for point-of-care testing (POCT) applications. The distinctive compartmentalization strategy of the pipette-operated dLAMP platform enables high scalability without compromising operational simplicity, achieving high throughput, wide dynamic range, and accurate quantification.

Received 17th May 2025,
Accepted 28th July 2025

DOI: 10.1039/d5lc00486a

rsc.li/loc

Introduction

Digital polymerase chain reaction (dPCR) is a powerful molecular diagnostic method that allows for the absolute quantification of nucleic acid target sequences with unprecedented sensitivity and precision without requiring a standard curve.[1–3] The principle of dPCR involves dividing a nucleic acid (DNA or RNA) sample into numerous discrete reaction partitions, such that each partition contains either zero, one, or more target molecules. Following amplification, the presence or absence of the target in each partition is detected, and then the absolute quantity of the target molecule in the original sample is determined by counting the number of positive partitions according to Poisson statistics.[4]

There are two principal methods for partitioning: droplet-based and chamber-based approaches. The droplet-based method[5–7] involves generating tens of thousands to millions of picolitre- to nanoliter-sized water-in-oil droplets using microfluidic technologies. This approach boasts several key advantages, including high partition numbers that enhance accuracy and dynamic range. In addition, microfluidic

[a] *Department of Mechanical Engineering, Toyohashi University of Technology, 1-1 Hibarigaoka, Tempaku-cho, Toyohashi, Aichi 441-8580, Japan. E-mail: shibata@me.tut.ac.jp*
[b] *Institute for Advanced Research (IAR), Nagoya University, Furo-cho, Chikusa-ku, Nagoya, Aichi 464-8601, Japan*
[c] *Department of Materials Process Engineering, Nagoya University, Furo-cho, Chikusa-ku, Nagoya, Aichi 464-8603, Japan*
[d] *Faculty of Pharmacy and Pharmaceutical Sciences, Josai University, 1-1 Keyakidai, Sakado, Saitama 350-0295, Japan*
[e] *Institute for Research on Next-generation Semiconductor and Sensing Science (IRES^2), Toyohashi University of Technology, 1-1 Hibarigaoka, Tempaku-cho, Toyohashi, Aichi 441-8580, Japan*

droplet generators used to produce emulsion droplets allow rapid and efficient partitioning, making them advantageous for high-throughput settings. However, this method also presents challenges, such as the requirement for costly specialized equipment to generate and analyze droplets and potential issues with droplet stability and uniformity, which can affect the accuracy of quantification.

The chamber-based method uses a fixed array of microchambers to generate physical compartmentalization. This includes different types of microfluidic formats, such as microchamber arrays integrated with active valves,[8] SlipChip,[9–11] microwell or microchamber arrays,[12–17] self-digitization (SD) chips,[18,19] and self-priming compartmentalization (SPC) chips.[20–25] This chamber-based approach offers the advantages of highly consistent and uniform partitions, reducing variability and improving reproducibility. Chamber-based dPCR systems typically require less complex instrumentation than droplet-based systems, potentially lowering operational costs and maintenance. Nonetheless, the number of partitions is limited to several hundred to a few thousand compartments, which can restrict the accuracy of quantification and the dynamic range of digital assays.[20] This limitation arises because precisely dispensing small volumes of liquid into numerous microchambers is technically challenging. In addition, uniform filling of these microchambers can be time-consuming, which may limit throughput. Several commercial dPCR systems are now available, each using different strategies for partitioning the sample.[3,4] However, commercial dPCR systems still have challenges, such as the high cost of instruments and consumables and the complexity of the equipment, which requires specialized training and expertise for optimal operation.

To overcome the limitations of dPCR, digital loop-mediated isothermal amplification (dLAMP) has emerged as a promising alternative for point-of-care testing (POCT) platforms.[26–29] LAMP operates under isothermal conditions (60–65 °C), in which a few copies of specific nucleic acid (DNA/RNA) targets can be amplified approximately 10^9–10^{10} times within 15–60 min using a set of four to six specifically designed LAMP primers.[30–32] This feature can obviate the need for the thermal cycling required in PCR, thus simplifying the equipment and operational procedures and offering robust solutions for a wide range of applications, from basic research to clinical diagnostics, food safety testing, and environmental pollutant monitoring. Similar to dPCR, the dLAMP method shares the principle of sample digitization, using either droplet-based methods[33–37] or chamber-based methods.[26] Among them, the chamber-based dLAMP approaches include SlipChip,[38–41] SD chip,[42–44] SPC chip,[45–48] microwell array with pneumatic valves,[49] and microchamber array with capillary burst valves.[50]

Lyu *et al.*[41] demonstrated digital reverse transcription LAMP (dRT-LAMP) for quantifying SARS-CoV-2 viral RNA using a modified SlipChip, called a droplet array SlipChip. This method involves manually sliding two glass plates, one with a high-density array of microwells and the other with a large loading channel and expansion chamber, to generate numerous discrete reaction partitions (21 698 wells of 0.25 nL each). The droplet array SlipChip eliminates the need for precise alignment, which was a limitation of the previous SlipChip. However, it requires manual operation, which demands skilled handling and is prone to human error, raising concerns regarding potential contamination. Kreutz *et al.*[43] applied a polydimethylsiloxane (PDMS)-based SD chip (1536 wells of 6.5 nL each) for the quantitative detection of human papillomavirus 18 (HPV-18) plasmid DNA using dLAMP. However, SD chips require complex and time-consuming operations, including priming the chip by filling it with oil to eliminate air, replacing the oil with an aqueous sample in the microwells, and isolating the aqueous sample by loading oil into the microfluidic channels. Zhang *et al.*[46] developed an improved SPC chip (980 wells of 18 nL each) for the detection *Staphylococcus epidermidis* infection using clinical aqueous humor samples. The SPC chip enables self-priming without external pumps, owing to the pre-degassed PDMS chip, which allows for the easy filling of an aqueous sample into microwells and subsequent separation by filling oil into the microchannel. However, the degassing state can change over time, posing challenges to the stability and reliability of the chip. In addition, the five-layer structure of the chip complicates the manufacturing process and potentially increases its cost. However, previous studies have not addressed techniques suitable for chamber-based dLAMP devices, which enable simple and rapid compartmentalization into tens of thousands of microwells. Lin *et al.*[50] developed a self-compartmentalization microfluidic device comprising microchambers connected to a main microchannel with three capillary burst valves (CBVs). By optimizing the relative burst pressures of the CBVs, the device successfully partitioned 12 800 dead-end chambers (0.9 nL each), with 83.8% of the chambers containing precisely 0.9 nL of the sample. To demonstrate the performance of the device, mock multiplex LAMP assays were successfully performed in a 144-chamber array (4 μL each). However, owing to the interdependent design constraints imposed on the three CBVs, including fixed burst pressure ratios and geometric coupling, it is inherently challenging to achieve both high-throughput operation and scalability within a single device architecture.

In our previous studies,[51–56] we developed a versatile microfluidic device for the multiplex detection of target nucleic acids based on the LAMP method. This technology has applications in a wide range of fields, including crop disease detection,[51] rapid identification of toxic plants for emergency medical care,[52] diagnosis of infectious diseases,[53,55] food allergen detection,[54] and foodborne pathogen detection.[56] The microfluidic device allows the sequential dispensing of sample/reagent mixtures into an array of reaction microchambers (3 μL each) in a single operation without surface coating, by exploiting the inherent hydrophobicity of the polymer. In addition, we developed a quantification system for nucleic acid targets by analyzing the color change in each reaction

microchamber from time-lapse images acquired during the LAMP reaction.[55,56] Furthermore, we proposed a parallel dilution microfluidic device with a four-stepwise logarithmic dilution capability for rapid and reliable detection of crudely extracted cannabis resin DNA.[57] This microfluidics-based system could be a platform for rapid and easy sample-to-answer diagnostics.

However, quantification of DNA concentration in samples still requires the prior generation of a standard curve, along with labor-intensive pipetting steps, to prepare a series of sample concentrations. Our previously developed sequential liquid dispensing method was limited to five to ten reaction microchambers, which was sufficient for our target genetic diagnostics. Therefore, in this study, we developed a high-speed sequential liquid compartmentalization method to realize a chamber-based dLAMP device with ten thousand microchambers, as a strong candidate for POCT platforms, enabling the absolute quantification of nucleic acid targets in a single test. Our proposed device enables the dead-end filling of ten thousand nanoliter-scale reaction microchambers while reliably eliminating air bubbles, with no methods commonly required in previously reported microfluidic devices, such as hydrophilic–hydrophobic coating to facilitate precise partitioning of the sample solution into individual microwells,[49] pre-priming with an immiscible oil to eliminate air,[43] or pre-degassing the PDMS device to remove trapped air.[46] Moreover, we demonstrated the absolute quantification of a foodborne pathogen (*Salmonella* spp.) and an illegal substance (*Cannabis sativa* L.) to validate the applicability of the fabricated dLAMP device. These two targets were intentionally chosen to represent distinct biological groups (bacteria and plants) and application fields (food safety and forensic science), highlighting the broad applicability of the platform across species and disciplines.

Experimental

Sequential liquid compartmentalization method

In our previous studies,[53,54,56] we proposed a theory for the sequential dispensing of liquid into multiple reaction microchambers by controlling the burst pressures of passive stop valves integrated within each microchamber. In this study, we investigated a newly designed valve configuration and structure to enable high-speed sequential liquid compartmentalization into ten thousand microchambers. Fig. 1 shows the schematic operation of the dLAMP device. Each microchamber was uniquely equipped with a set of three valves: a temporary stop valve (S_1) and two permanent stop valves (S_2 and S_3). The partitioning procedure operates as follows: first, the flow of the aqueous sample solution (a mixture of DNA sample and LAMP reagents) in the main microchannel is stopped at the temporary stop valve S_1 (designed with burst pressure P_1) owing to the surface tension of the liquid and redirected toward the microchamber (Fig. 1a). Once the microchamber is filled, the liquid flow is stopped by the permanent stop valve S_2 (designed with burst pressure P_2). Valve S_2 helps exhaust air in the microchamber through an air-vent microchannel. Subsequently, the liquid flows toward the next microchamber by passing through valve S_1 because $P_1 < P_2$. Furthermore, the burst pressure of valve S_2 substantially increased after an air plug was trapped between valve S_2 and permanent stop valve S_3 (Fig. 1b). This valve configuration was developed based on a modified version of the air plug-in valve described in our previous studies.[54,56] This process was replicated to sequentially fill all the microchambers. Following sample loading, oil was introduced into the microchannel to isolate the solution within each reaction microchamber, preventing cross-contamination and enabling compartmentalized LAMP reactions (Fig. 1c). After performing gene amplification at a constant temperature (Fig. 1d), the absolute quantity of the target DNA molecules (C) in the original sample is determined by counting the number of positive microchambers (b), according to Poisson statistics as follows:[26]

$$C = -\ln\left(1 - \frac{b}{n}\right)/V \quad (1)$$

where n is the total number of microchambers and V is the microchamber volume.

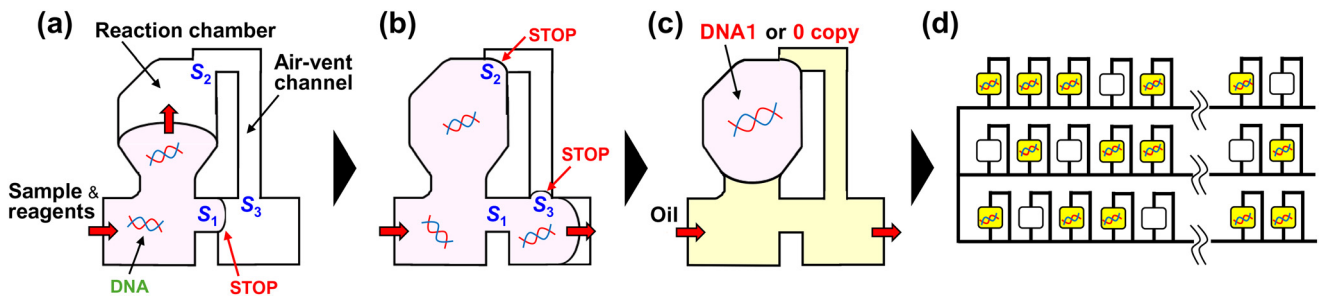

Fig. 1 Operating principle of a digital LAMP device. (a) A mixture of DNA sample and LAMP reagents was introduced. (b) After the microchamber is filled with liquid, it flows toward the second microchamber. (c) Introduction of the separated oil phase for partitioning. (d) After heating and performing gene amplification, the number of positive microchambers is measured to determine the absolute quantity of target DNA molecules in the original sample.

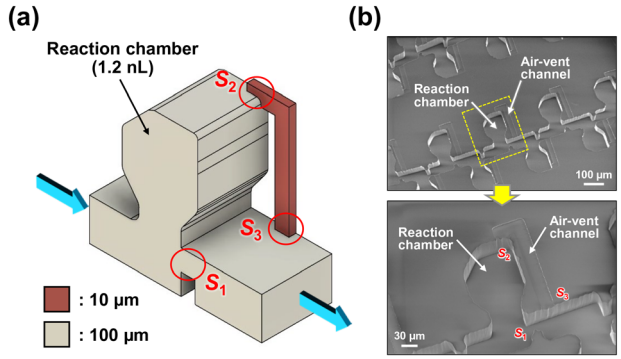

Fig. 2 Schematic diagram of a reaction microchamber for sequential liquid partitioning. (a) Detailed design of the microchamber structure showing the valve configuration and layout of the air-vent microchannel. (b) Scanning electron microscopy images of the fabricated PDMS-based microchamber connected to a 100 μm-high main microchannel and a 10 μm-high air-vent microchannel.

Design and fabrication of microchamber integrated with a set of three passive stop valves and an air-vent microchannel

Fig. 2a shows a schematic of the reaction microchamber integrated with a set of three valves: a temporary stop valve (S_1) and two permanent stop valves (S_2 and S_3). A design feature is that only the air-vent microchannel (width: 20 μm) is fabricated with a height of 10 μm, whereas all other microchannels (width: 60 μm) and microchambers (volume: 1.2 nL) are 100 μm in height. The detailed geometrical dimensions are presented in Fig. S1. The theoretical burst pressures of the S_1, S_2, and S_3 valves were designed to be P_1 = 3.07, P_2 = 5.42, and P_3 = 6.03 kPa for water (surface tension γ = 0.073 N m^{-1}), according to the theoretical model described in our previous study.[54]

To investigate the sequential liquid compartmentalization process, a polydimethylsiloxane (PDMS)-based microfluidic device with 100 reaction microchambers arranged in series (Fig. S1) was fabricated using a soft lithography process. The fabrication process is briefly described as follows: first, a negative thick photoresist (SU-8 3010; MicroChem, Newton, MA, USA) was patterned on a 4 inch single-crystal silicon (Si) wafer (e-Prize, Yokohama, Japan) for the first layer with a thickness of 10 μm through a photolithography process, patterning the air-vent microchannels. Next, the second layer with a thickness of 90 μm was patterned on the same Si wafer using a higher-viscosity negative thick photoresist (SU-8 3050) to form molds for the microchambers and microchannels, resulting in a total structure height of 100 μm. Subsequently, the SU-8 master mold was replicated in PDMS (Silpot 184; Dow Corning Toray, Tokyo, Japan) after curing on a hotplate at 85 °C for 40 min. After peeling off the PDMS from the SU-8 master mold, circular holes for the inlet and outlet ports (with a diameter of 1.0 mm) were punched into the PDMS microfluidic device using a biopsy punch piercing tool (Kai Industries, Gifu, Japan). Finally, the microchambers and microchannels on the PDMS surface were sealed with a glass plate (S9213; Matsunami Glass, Osaka, Japan) using a silicone-based adhesive double-sided tape (no. 5303 W; Nitto Denko, Osaka, Japan).

Fig. 2b shows images of the fabricated PDMS-based microchambers integrated with a set of three valves and an air-vent microchannel acquired using a scanning electron microscope (GeminiSEM 560; ZEISS, Jena, Germany). Downstream of the inlet to the reaction microchamber (100 μm in height; 1.2 nL in volume), valve S_1 with a 30 μm gap was fabricated in the main microchannel (60 μm wide and 100 μm high). In addition, the air-vent microchannel (60 μm wide and 10 μm high) was precisely aligned and connected to the reaction microchamber and the main microchannel, forming valves S_2 and S_3, respectively.

Investigation of the sequential liquid compartmentalization process

To investigate the liquid compartmentalization process in a device with 100 reaction microchambers, red-colored water and fluorinated oil (Fluorinert™ FC-40; 3M, St. Paul, MN, USA) were used as the aqueous and oil phases, respectively. The volumetric flow rate was controlled using a syringe pump (YSP-201, YMC, Kyoto, Japan) to introduce liquids into the devices. In the experiments, a 1 mL syringe was first filled with 0.7 mL of oil and connected to a polyvinyl chloride (PVC) tube (inner diameter: 0.55 mm). After the tube was primed with oil up to its tip, 20 μL of colored water was subsequently aspirated into the tube from the tip. The tube was then inserted into the inlet port of the device, and colored water, followed by oil, was sequentially introduced into the microchannel. The flow behaviors of the two liquids were observed using an inverted microscope (ECLIPSE Ti2-U; Nikon, Tokyo, Japan) equipped with a high-speed complementary metal-oxide semiconductor (CMOS) camera (HAS-D71M; DITECT, Tokyo, Japan).

Sample preparation and fluorescent LAMP reagents

The LAMP primers for detecting *Salmonella* spp. and *Cannabis sativa* L. were designed based on previous reports.[58,59] Because *Salmonella* spp. requires handling at biosafety level 2, *Salmonella* DNA templates (401 bp) for LAMP detection were synthesized using artificial oligonucleotides (Eurofins Genomics, Tokyo, Japan). Similarly, cannabis DNA templates (218 bp) targeting the tetrahydrocannabinolic acid (THCA) synthase gene were synthesized for LAMP detection (Eurofins Genomics). THCA is decarboxylated to form tetrahydrocannabinol (THC), which is responsible for strong psychoactive effects. The LAMP primer and synthetic template sequences for *Salmonella* and cannabis are listed in Tables S1[58] and S2,[59] respectively. For comparison with these synthetic templates, genomic cannabis DNA templates were prepared by extracting genomic DNA from purified cannabis seeds (purchased from Uchida Wakanyaku, Tokyo, Japan) using the FavorPrep Plant Genomic DNA Extraction Mini Kit (Chiyoda Science, Tokyo, Japan). DNA concentrations were quantified using a Qubit 4 Fluorometer and Qubit dsDNA HS

Assay Kit (Thermo Fisher Scientific, Waltham, MA, USA) and adjusted to the final concentrations required for the experiments. In addition, to evaluate amplification performance in the presence of inhibitors, humic acid[60] (FUJIFILM Wako Pure Chemical, Osaka, Japan)—a major DNA amplification inhibitor and one of the main decomposition products of plant and animal matter found in soil—was added to the sample/reagent mixture at concentrations ranging from 1 to 15 ng μL^{-1}.

LAMP reactions were performed using the Loopamp® DNA amplification kit (Eiken Chemical, Tokyo, Japan), which includes a 2× reaction mix and thermostable *Bst* polymerase. Fluorescence-based detection was enabled using the Loopamp® fluorescent detection reagent (Eiken Chemical), which comprises calcein and manganese chloride ($MnCl_2$). In the LAMP reaction, manganese ions (Mn^{2+}) quench calcein fluorescence. As amplification proceeds, the pyrophosphate ions produced as a reaction byproduct bind to Mn^{2+} ions, releasing calcein and restoring fluorescence. Subsequently, magnesium ions (Mg^{2+}) in the reaction mixture bind to free calcein, further enhancing the fluorescent signal.[48] The final mixture volume was 25 μL, comprising the nucleic acid sample, LAMP reagents, fluorescent detection reagent, and primer sets (1.6 μM of inner primers (FIP and BIP), 0.2 μM of outer primers (F3 and B3), and 0.8 μM of loop primers (LF and LB)), which was prepared for fluorescent LAMP assays in the digital LAMP device (Table S3). Before the experiments, the DNA template and primers were denatured at 85 °C for 3 min to enhance amplification efficiency.[41,49] After cooling to room temperature, the LAMP reagents and fluorescent detection reagent were mixed and loaded into the dLAMP device. For comparison, LAMP assays using synthetic cannabis DNA templates targeting the THCA synthase gene (Table S4) and cannabis seed samples with the addition of humic acid (Table S5) were conducted off-chip in 0.2 mL PCR tubes (25 μL reaction volume) using a real-time turbidimeter (LoopampEXIA; Eiken Chemical). The same Loopamp® DNA amplification kit was used for the assays.

Operating procedure for the on-chip fluorescent LAMP assay

To evaluate its applicability to the digital LAMP method, a PDMS-based microfluidic device with 10 000 reaction microchambers was fabricated (Fig. S2). The device comprised 10 rows, each containing 1000 microchambers connected in a series. To achieve a compact design, the microchambers were alternately arranged on both sides of the main microchannel, allowing the entire device to fit within a 40 mm square. This compact layout also shortened the main microchannel length, reducing the overall flow resistance of the device. In addition, all 10 rows were designed to have identical microchannel lengths by incorporating serpentine microchannels of appropriate lengths after the main microchannel branches. This design ensured simultaneous liquid inflow across all rows upon sample and oil introduction during partitioning.

In the LAMP assays, to simplify the operation and minimize the risk of contamination, the aqueous sample solution (a mixture of DNA sample and LAMP reagents) and fluorinated oil were introduced into the device using a custom electronic pipette (pipetty 250 μL; Icomes Lab, Iwate, Japan) instead of a syringe pump. The experimental procedure was as follows: first, 100 μL of oil was aspirated into a 200 μL pipette tip attached to an electronic pipette, followed by 15 μL of sample solution. The tip was inserted into the device's inlet port; subsequently, the sample solution and oil were loaded sequentially. After all microchambers were compartmentalized, the inlet and outlet ports were sealed with silicone-based double-sided tape and mechanically clipped between two glass plates placed on both sides of the device. The assembly was then placed in a hot-water bath (TB-1NC; AS ONE, Osaka, Japan) to facilitate the amplification of the targeted nucleic acids *via* the LAMP reaction under stable isothermal conditions at 60 °C for 60 min for *Salmonella* and 63 °C for 60 min for cannabis seeds.

Quantification of DNA concentrations in the samples

After the LAMP assays, the fluorescence intensity of each reaction microchamber was analyzed using a fluorescence microscope (BZ-X810; Keyence, Osaka, Japan). The fluorescence threshold was defined as $\bar{x} + 4\sigma$ (where $\bar{x}$ and σ are the mean and standard deviation, respectively) of the fluorescence intensity in the negative control, which was conducted on the device by heating the LAMP reagents except for DNA template at a specific temperature (60 °C for *Salmonella* and 63 °C for cannabis seeds) for 60 min. The number of microchambers with fluorescence intensities exceeding this threshold was counted as a positive reaction. To quantify the DNA concentration based on eqn (1), the mean volume of the sample solution compartmentalized in each microchamber before heating was used. This volume was calculated as the product of the measured fluorescent area and the measured microchamber height (approximately 100 μm) for each sample.

Results and discussion

Characterization of the compartmentalization method

Fig. 3 shows the liquid partitioning process when colored water, followed by oil, was introduced into the device with 100 microchambers (1.2 nL each) connected in series (Fig. S1) at a flow rate of 100 $\mu L\ min^{-1}$, using a syringe pump. As described in the operating principle, the colored water flowing through the main microchannel stopped at valve S_1 and then flowed into the microchamber. Once the microchamber was filled and the liquid reached valve S_2, the liquid flowed toward the next microchamber by passing through valve S_1. In addition, air was trapped in the air-vent microchannel between valves S_2 and S_3, forming an air plug-in valve.[54,56] This process was repeated, resulting in the complete dispensing of liquid into all microchambers.

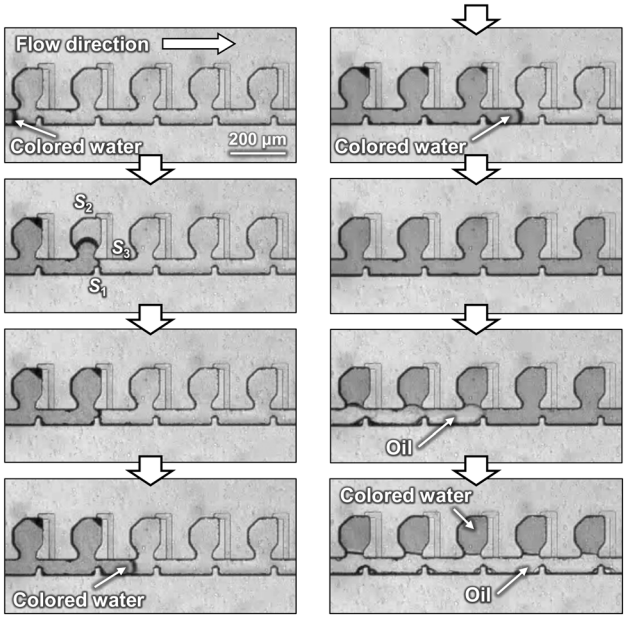

Fig. 3 Experimental results showing the liquid partitioning process in a device with 100 microchambers (1.2 nL each). Colored water was introduced first, followed by oil at a flow rate of 100 μL min^{-1}.

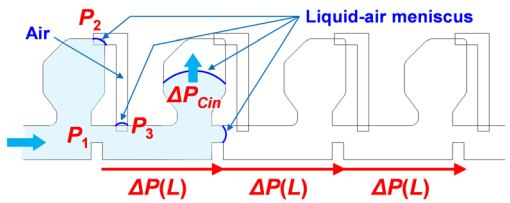

Fig. 4 Sequential liquid dispensing model using the air plug-in valve. After the first microchamber is filled, the liquid flow is halted at the valve S_1 of the second microchamber, initiating its filling.

Subsequently, oil inflow isolated the colored water within each microchamber. The total time required for the compartmentalization of all 100 microchambers was only 0.34 s (equivalent to 300 chambers per s). However, the unexpected leakage of colored water through valves S_2 and S_3 into the air-vent microchannel was observed (Video S1). This valve leakage behavior is based on the theory for sequential liquid dispensing using the air plug-in valve, as proposed in our previous studies.[54,56]

Fig. 4 shows the liquid dispensing model. After the first microchamber was filled, the liquid flow was temporarily halted at valve S_1 of the second microchamber, initiating the filling process. At this stage, valve S_2 of the first microchamber is subjected to three pressure components: the burst pressure P_1, the pressure required to flow the liquid through the main microchannel over a length L between the first and second microchambers, and the pressure required for the liquid to fill the microchamber (denoted as ΔP_{Cin}). The pressure $P(S_2)$ applied to valve S_2 of the m-th microchamber during dispensing into the n-th microchamber can be expressed as:

$$P(S_2) = P_1 + (n - m)\Delta P(L) + \Delta P_{Cin} \quad (2)$$

Similarly, the applied pressure $P(S_3)$ acting on valve S_3 is expressed as:

$$P(S_3) = (n - m)\Delta P(L) + \Delta P_{Cin} \quad (3)$$

As the number of filled microchambers increased, the pressure required to flow the liquid through the main microchannel also increased. These pressures can readily exceed the burst pressures of valves S_2 and S_3, resulting in liquid leakage into the air-vent microchannel. To address this issue, air is intentionally trapped between valves S_2 and S_3 to offset the pressures applied to each valve because the liquids reaching the two valves push against each other through an air plug. Only the differential pressure (denoted as ΔP_{offset}) given by the following equation was applied to valves S_2 and S_3, significantly enhancing their pressure-resistance performance:

$$\Delta P_{offset} = P(S_2) - P(S_3) = P_1 \quad (4)$$

Thus, in theory, rupture of these valves does not occur because the burst pressures of valves S_2 and S_3 (P_2 and P_3, respectively) are consistently designed to exceed those of valve S_1 (P_1). However, owing to the inherent gas permeability of PDMS,[54] the air plug trapped within the air-vent microchannel gradually leaks out under elevated internal pressure, eventually allowing liquid to intrude into the air-vent microchannel. Nevertheless, the key advantage of the present design is that even if a liquid enters the air-vent microchannel, it can still be successfully isolated by the subsequent introduction of oil.

To compare the performance of liquid compartmentalization with that of the device shown in Fig. 2a, the height of the air-vent microchannel was set to 100 μm (Fig. S3 and Video S2). Each microchamber had a volume of 0.84 nL, and the theoretical burst pressures of valves S_1, S_2, and S_3 were designed to be approximately equal: P_1 = 3.07, P_2 = 6.67, and P_3 = 5.41 kPa for water, respectively. As expected, the colored water was successfully dispensed into all microchambers. However, like the previous results (Fig. 3 and Video S1), valves S_2 and S_3 ruptured, allowing water to intrude into the air-vent microchannel. Subsequently, upon the introduction of oil, it flowed into the microchambers, resulting in the failure of compartmentalization. The theoretical flow resistance of the air-vent microchannel with a height of 100 μm for water (dynamic viscosity η = 1 mPa s) was calculated to be 0.04 kPa min μL^{-1}, which is approximately 90 times lower than the air-vent microchannel with a height of 10 μm (3.73 kPa min μL^{-1}). The calculation method for the flow resistance is detailed in our previous study.[54] This suggests that the water in the microchambers was pushed into the main microchannel through the air-vent microchannel by the pressure of the oil. This comparative experiment further demonstrated that increasing the flow resistance of the air-

vent microchannel is critical for preventing water displacement from the microchambers through the air-vent microchannel. An air-vent microchannel was designed to function as a secondary flow resistor, acting as a passive valve to control liquid displacement, which is a key feature that distinguishes our approach. Therefore, the proposed structure is essential for achieving reliable and high-speed liquid compartmentalization.

Implementation of the compartmentalization method in the digital LAMP device

Fig. 5a shows the liquid partitioning process when colored water (20 μL), followed by oil (100 μL), was introduced into the device with 10 000 microchambers (1.2 nL each) at a flow rate of 100 μL min^{-1}. As expected, the liquids (water followed by oil) were introduced nearly simultaneously into all 10 main microchannels connected in parallel, resulting in almost simultaneous completion of compartmentalization (Video S3). As shown in Fig. 5b, the liquid was successfully isolated in microchambers that were alternately arranged on both sides of the main microchannel. The total time required to compartmentalize all 10 000 microchambers was only 25 s, corresponding to a throughput of approximately 400 chambers per s. As additional information, we measured the time required to fill five consecutive segments of 200 microchambers each, corresponding to 1000 microchambers in the sixth row of serpentine microchannels out of 10 arranged in parallel. As shown in Fig. S4, the filling times across the five positions were consistent, with an average of 2.2 s and a standard deviation of 0.2 s. The total time required to fill 1000 microchambers with the aqueous solution alone (before oil introduction) was approximately 11 s.

In the LAMP experiments, to simplify the operation and minimize the risk of contamination, the aqueous sample solution (a mixture of DNA sample and LAMP reagents) and fluorinated oil were introduced into the device using a custom electronic pipette instead of a syringe pump (Video S4). Owing to the characteristics of the electronic pipette, precise control of the flow rate was not feasible, since the discharge speed decreased as the liquid volume remaining in the pipette tip decreased.[55] As shown in Fig. S4, the filling time increased markedly beyond the third turning point along the serpentine microchannel. The total time required to fill 1000 microchambers with the aqueous solution alone (before oil introduction) was approximately 21 s, which was approximately twice as long as that with the syringe pump. Although the total compartmentalization time increased to approximately 60 s, a high throughput of approximately 170 chambers per s was maintained. In this experiment, the actual sample/reagent mixtures used for the LAMP assays were introduced into the device, except for the addition of colored water for visualization, demonstrating successful compartmentalization under realistic conditions.

Fig. 6 shows a representative experimental result of the measured volumes of a sample/reagent mixture compartmentalized in the individual reaction microchambers of the dLAMP device using an electronic pipette. The correspondence between the chamber number on the *x*-axis and the device layout is shown in Fig. S5. To determine the volumes, the fluorescent area measured using a fluorescence microscope was multiplied by the height of the microchamber (approximately 100 μm). A microscopy image of the 10 000 reaction microchambers is shown in Fig. S6.

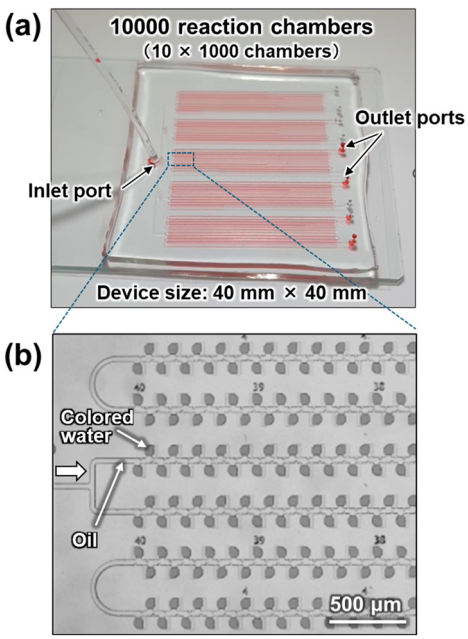

Fig. 5 A fabricated PDMS-based digital LAMP device with 10 000 microchambers arranged in 10 rows, each containing 1000 microchambers connected in series. (a) Photograph of the device showing the colored water compartmentalized by oil. (b) Close-up view after compartmentalization showing microchambers alternately arranged on both sides of the main microchannel.

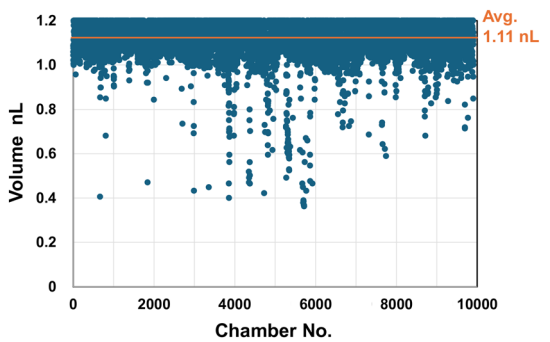

Fig. 6 Representative results showing the measured volumes of a sample/reagent mixture compartmentalized into individual reaction microchambers using an electronic pipette. Of the 10 000 microchambers, of the 10 000 microchambers, 9667 (97%) were successfully compartmentalized with a filling ratio of ≥80% (≥0.96 nL). The average compartmentalized volume was 1.11 ± 0.08 nL (CV = 0.07). The microchambers were filled to 93% of their designed volume (1.2 nL).

Incomplete air removal in some microchambers led to either the absence of liquid introduction or insufficient liquid volume. However, 9667 out of 10 000 reaction microchambers were successfully compartmentalized with a filling ratio of ≥80% (≥0.96 nL) of their designed volume, corresponding to a 97% success rate. The average compartmentalized volume was 1.11 ± 0.08 nL (coefficient of variation CV = 0.07), indicating that the microchambers were filled with liquid to 93% of their designed volume (1.2 nL). This result demonstrates that the sample/reagent mixture was compartmentalized with a high precision. As SI, Fig. S7 shows the number of microchambers filled above a filling ratio of ≥80% (≥0.96 nL) for each of the ten parallel serpentine microchannels (1000 chambers per channel). Although rows 4–6 exhibited a modest decrease in the number of sufficiently filled microchambers, the difference was only 3%, which is not substantial enough to indicate any considerable positional trend regarding the microchannel placement within the device.

Fluorescent LAMP assay in the digital LAMP devices

Fig. 7a shows fluorescence microscopy images of 10 000 reaction microchambers of the dLAMP devices after running the assay at 60 °C for 60 min to detect synthetic *Salmonella* DNA templates at a concentration of 10^{-2} ng μL^{-1} (2.3×10^7 copies per μL). Almost all the reaction microchambers exhibited green fluorescence, indicating a positive reaction. However, some microchambers were unexpectedly found to be interconnected *via* a main microchannel. In this study, these microchambers were excluded from the count of valid chambers used for absolute quantification because of possible the cross-contamination. In our previous study,[56] we reported that residual air remaining in the microchamber after dispensing a sample/reagent mixture may act as nuclei for the growth of air bubbles during the LAMP assay, possibly because of residual air diffusing from the PDMS. One explanation for this unexpected behavior is that the oil in the main microchannel was pushed away by expanding air bubbles originating from the microchambers, allowing the leaked mixture to flow into the main microchannel and causing interconnections between neighboring microchambers. Further investigation is required to elucidate the underlying causes. In the future, we plan to use plastic-based devices with lower gas permeability. Preliminary studies have already demonstrated successful LAMP amplification on plastic devices without the inhibitory effects of surface adsorption. In addition, we confirmed that the autofluorescence of the plastic material used was sufficiently low, posing no issue as background noise for fluorescence-based detection. As the DNA concentration decreased to 10^{-4} ng μL^{-1} (2.3×10^5 copies per μL) (Fig. 7b), the number of microchambers exhibiting positive reactions decreased. Furthermore, when the DNA concentration reached 10^{-6} ng μL^{-1} (2.3×10^3 copies per μL) (Fig. 7c), almost all the microchambers exhibited negative results.

Fig. 8 shows the relationship between the DNA concentration in the sample and the DNA concentration quantified from the experimental results. The experiments were conducted under five DNA concentration conditions.

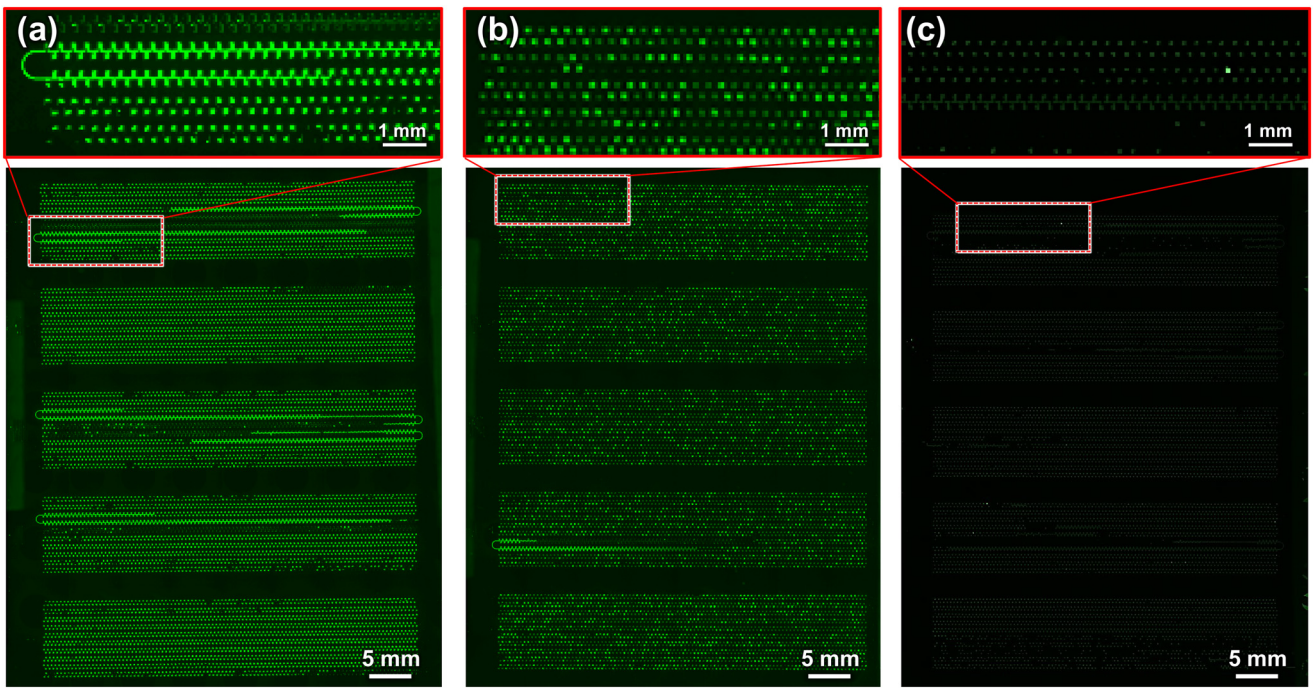

Fig. 7 Fluorescent LAMP assay using digital LAMP devices. Fluorescence microscopy images of 10 000 reaction microchambers after running the assays at 60 °C for 60 min for the detection of synthetic *Salmonella* templats at DNA concentrations of (a) 10^{-2} ng μL^{-1} (2.3×10^7 copies per μL), (b) 10^{-4} ng μL^{-1} (2.3×10^5 copies per μL), and (c) 10^{-6} ng μL^{-1} (2.3×10^3 copies per μL).

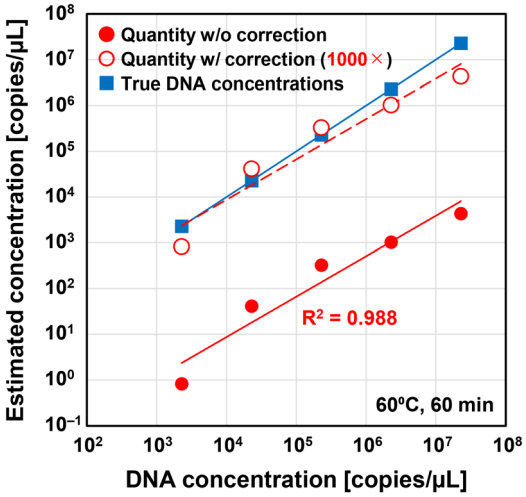

Fig. 8 Relationship between the DNA concentrations in the synthetic *Salmonella* templates and the quantification results obtained from the digital LAMP devices.

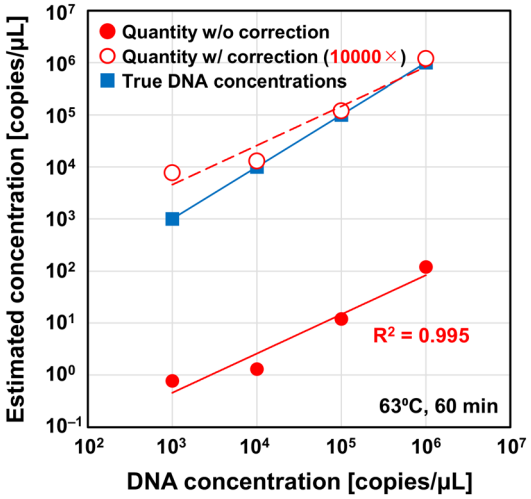

Fig. 9 Relationship between the DNA concentrations in the synthetic cannabis templates tageting THCA synthase gene and the quantification results obtained from the digital LAMP devices.

Table S6 summarizes the number of measured chambers, positive chambers, and percentage of positive chambers. The fluorescence intensity distributions of the reaction microchambers obtained at each DNA concentration are shown in Fig. S8. The fluorescence threshold for determining a positive reaction was set at a value of 27, based on the histogram of fluorescence intensities of the negative control ($\bar{x}$ = 17.0 and σ = 2.3), as described in the Experimental section. The red solid circles in the graph represent the estimated DNA concentrations in the sample using eqn (1), showing a strong positive correlation (coefficient of determination R^2 = 0.988). However, the experimentally estimated DNA concentrations, based on the number of chambers showing positive reactions, was underestimated compared to the true DNA concentrations (represented by blue solid squares). Nevertheless, the similar slope between the experimental and true values suggests that the experimental results accurately reflected the sample DNA concentration. The red open circles in the graph represent the values calculated using eqn (1) with a correction factor of 1000. Compared to the uncorrected values (represented by red solid circles), the corrected values more closely approximate the true DNA concentrations. This result suggests that, in this experiment, microchambers containing 1000 or more DNA copies exhibited positive results. Our previous experimental results showed the limit of detection (LOD) of 1000 copies per μL for *Salmonella*,[56] which is consistent with the results obtained in this study. However, the principle of absolute quantification in digital LAMP requires a positive reaction even if a single DNA copy is present in a microchamber. Therefore, these results indicate that the current detection sensitivity is inadequate.

Fig. 9 shows the relationship between the DNA concentration in the sample and the DNA concentration quantified from the assay at 63 °C for 60 min in the digital LAMP devices for the detection of synthetic cannabis templates with DNA concentrations ranging from 2.5×10^{-4} ng μL^{-1} (1.0×10^6 copies per μL) to 2.5×10^{-7} ng μL^{-1} (1.0×10^3 copies per μL). Table S7 summarizes the number of measured chambers, positive chambers, and percentage of positive chambers. The estimated DNA concentrations in the samples (red solid circles) showed a strong positive correlation (coefficient of determination R^2 = 0.995). However, a correction factor of 10 000 was required to approximate the true DNA concentrations (red open circles), which was 10 times higher than that required for *Salmonella*. Despite this discrepancy, the LOD was approximately 10^3 copies per μL, comparable to that observed for *Salmonella*. In contrast, off-chip turbidity measurements (25 μL reaction volume) yielded a higher LOD of approximately 10^6 copies per μL (Fig. S9). Although the underlying reason remains unclear, these findings suggest that the digital LAMP method

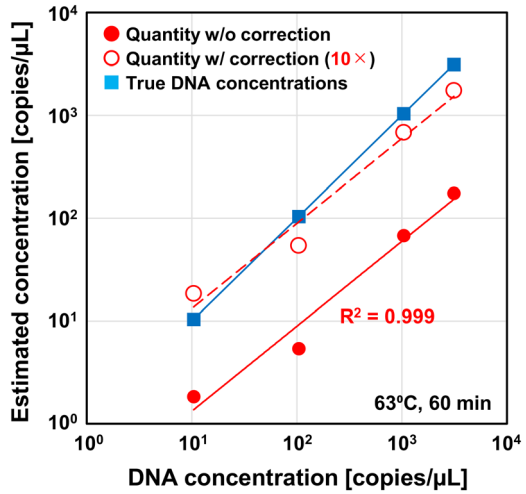

Fig. 10 Relationship between the DNA concentrations in the purified cannabis seed samples and the quantification results obtained from the digital LAMP devices.

may offer improved detection sensitivity compared with turbidity-based approaches.

To evaluate the applicability of the digital LAMP device to natural samples, digital LAMP assays were conducted at 63 °C for 60 min using DNA templates purified from cannabis seeds with DNA concentrations ranging from 3 ng μL^{-1} (3.1×10^3 copies per μL) to 10^{-2} ng μL^{-1} (1.0×10^1 copies per μL). Fig. 10 shows the relationship between the DNA concentration in the sample and the DNA concentration quantified using the assay. The numbers of measured chambers, positive chambers, and percentages of positive chambers are summarized in Table S8. The estimated DNA concentrations (red solid circles) exhibited a strong positive correlation (R^2 = 0.999) and a slope similar to that of the true DNA concentrations (blue solid squares). Despite using the same primer set as in the synthetic cannabis assay, the required correction factor was reduced to 10 to be consistent with the true values (red open circles), which was notably smaller than the factors of 1000 and 10 000 used in the synthetic *Salmonella* and cannabis assays, respectively. Our previous experimental results showed an LOD of 10 copies per μL for cannabis seeds,[57] which is consistent with the results obtained in this study.

The difference in correction factors between the digital LAMP experiments for the three types of DNA templates suggests that the quantification differences are primarily due to the intrinsic performance of the LAMP assays rather than the characteristics of the PDMS device. The primary factor contributing to this marked difference in LODs is likely because of a combination of the intrinsic sensitivity and performance of the respective LAMP primer sets and the characteristics, including type and length, of the template DNA. In LAMP, the initial formation of a dumbbell-like DNA structure by inner primers (FIP and BIP) is critical for initiating amplification.[30] The ability of a primer to form this structure depends not only on its binding to the target sequence but also on its capacity to invade the template strand and adopt conformations that favor loop formation and self-priming. Recent studies have demonstrated that stable secondary structures within the single-stranded regions of FIP or BIP can hinder strand invasion and proper annealing, reducing the efficiency of dumbbell formation.[61] This structural susceptibility may partly explain the relatively lower amplification efficiency observed with the *Salmonella*-specific and cannabis-specific primer sets in this study. Considering that the correction factor was 1000 for the LAMP reaction using the 401 bp synthetic *Salmonella* template DNA and 10 000 for the reaction using the 218 bp cannabis template DNA, it is possible that non-target DNA is required to achieve optimal amplification efficiency in LAMP. Given that genomic DNA extracted from natural cannabis seeds was used, non-target DNA may have induced instability in the secondary structures within the single-stranded regions of the FIP or BIP primers, potentially enhancing the detection sensitivity. In addition, the LAMP assay targeting purified cannabis DNA was designed to amplify the THCA synthase gene, which exists in multiple copies within the genome, potentially resulting in increased detection sensitivity.[62] The results suggest that the amplification efficiency in LAMP is not solely determined by the presence of the target sequence, but is also influenced by other factors such as primer-template interaction dynamics, template length, and secondary structure formation. However, the need for a correction factor undermines a key advantage of the digital LAMP method: its ability to perform absolute quantification without a standard curve. Therefore, further investigation should focus on understanding the impact of primer design and template characteristics on the quantification accuracy.

To investigate the influence of gene amplification inhibitors, we assessed the performance of a digital LAMP device using purified cannabis seed DNA in the presence of humic acid. As a preliminary step, the inhibitory effect of humic acid at concentrations ranging from 1 to 15 ng μL^{-1} was assessed using conventional off-chip real-time turbidity measurements (25 μL reaction volume). As shown in Fig. S10, the amplification reaction was inhibited at a concentration of 5 ng μL^{-1}, with more pronounced inhibitory effects observed at lower DNA template concentrations. Furthermore, when the concentration of humic acid was increased to 10 ng μL^{-1}, no detectable amplification occurred. These findings align with earlier study results.[60] Based on these results, humic acid at 10 ng μL^{-1} was applied in subsequent digital LAMP assays. Fig. 11 shows the estimated DNA concentrations in the sample (red solid circles). Table S9 summarizes the number of measured microchambers, the number of positive chambers, and the percentage of positive reactions. A comparison with the results obtained in the absence of humic acid (green solid circles) revealed that the digital LAMP device exhibited strong tolerance to amplification inhibitors, as the quantitative performance remained largely unaffected. These results demonstrate the applicability of the digital LAMP device to real-world samples

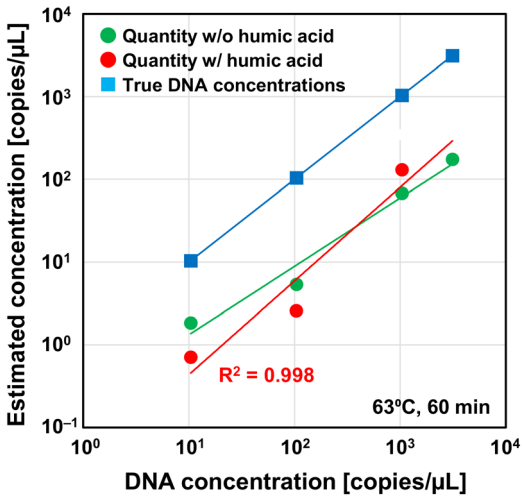

Fig. 11 Relationship between the DNA concentrations in the purified cannabis seed samples with humic acid and the quantification results obtained from the digital LAMP devices.

and environments, supporting its potential as a viable platform for POCT applications.

Conclusions

In this study, we developed a high-speed sequential liquid compartmentalization method for a digital LAMP platform based on a chamber-based microfluidic approach, eliminating the need for complex procedures such as surface modification, pre-degassing of the PDMS device, pre-priming with immiscible oil, or external pumping systems. A distinctive feature of the digital LAMP device is that each microchamber incorporates a set of three passive stop valves and an air-vent microchannel with significantly high flow resistance, achieved by reducing the height of the microchannel. This design enables reliable sample dispensing and oil-based compartmentalization. The fabricated PDMS device successfully achieved rapid and uniform dead-end filling of 10 000 reaction microchambers (each with a volume of 1.2 nL) within 60 s in a single pipetting operation, using an electronic pipette to sequentially introduce an aqueous sample/reagent mixture, followed by fluorinated oil. The experimental results demonstrated that 97% of the microchambers were filled to at least 80% of their designed volume with high-volume uniformity (CV = 0.07). Furthermore, the pipette-operated digital LAMP strategy facilitates operational simplicity and minimizes contamination risk, which is essential for practical molecular diagnostic applications.

Fluorescent LAMP assays targeting *Salmonella* and cannabis showed strong linearity between estimated and true DNA concentrations ($R^2 > 0.98$), confirming the quantitative capability of the device. However, correction factors were required to match the true values—1000 and 10 000 for synthetic DNA templates of *Salmonella* and cannabis, respectively, and only 10 for DNA extracted from cannabis seeds—indicating that the quantification accuracy is primarily affected by the intrinsic performance of the LAMP assays rather than the device performance. Possible contributing factors are that primer performance and template characteristics remain key limitations in achieving absolute quantification. Furthermore, the dLAMP device successfully detected cannabis seed DNA even in the presence of 10 ng μL^{-1} humic acid, a known inhibitor that suppresses amplification in conventional turbidity-based LAMP assays, demonstrating its robustness and suitability for POCT applications. Future studies will aim to further optimize assay components, including primer design, template quality, and reaction conditions, and evaluate device performance using crude DNA extracts containing diverse amplification inhibitors to validate its utility in clinical and field-based molecular diagnostics.

Author contributions

Riku Honda; methodology, investigation, writing – original draft preparation, Taketo Saruwatari; methodology, investigation, Daigo Natsuhara; methodology, investigation, writing – review and editing, Yuka Kiba; methodology, investigation, Shunya Okamoto; writing – review and editing, supervision, Moeto Nagai; writing – review and editing, supervision, Masashi Kitamura; methodology, writing – review and editing, supervision, Takayuki Shibata; conceptualization, methodology, writing – review and editing, supervision, project administration, funding acquisition. All authors have read and agreed to the published version of this manuscript.

Conflicts of interest

The authors declare no conflicts of interests.

Data availability

Supplementary information is available: The Supplementary Information includes detailed designs of microfluidic devices, experimental conditions for LAMP assays, additional experimental results presented in figures and tables, and movies demonstrating the liquid compartmentalization process. See DOI: **https://doi.org/10.1039/D5LC00486A**.

The authors confirm that the data supporting the findings of this study are available within the main article and SI.

Acknowledgements

This research was partially supported by JSPS KAKENHI Grant Number JP24K00776. We would like to thank Editage (**http://www.editage.com**) for the English language editing.

References

1 B. Vogelstein and K. W. Kinzler, *Proc. Natl. Acad. Sci. U. S. A.*, 1999, **96**, 9236–9241, DOI: **10.1073/pnas.96.16.9236**.
2 X. Xiang, Y. Shang, J. Zhang, Y. Ding and Q. Wu, *TrAC, Trends Anal. Chem.*, 2022, **149**, 116568, DOI: **10.1016/j.trac.2022.116568**.
3 Y. Ren, L. Cao, M. You, J. Ji, Y. Gong, H. Ren, F. Xu, H. Guo, J. Hu and Z. Li, *TrAC, Trends Anal. Chem.*, 2022, **157**, 116774, DOI: **10.1016/j.trac.2022.116774**.
4 A. S. Basu, *SLAS Technol.*, 2017, **22**, 369–386, DOI: **10.1177/2472630317705680**.
5 D. Xu, W. Zhang, H. Li, N. Li and J.-M. Lin, *Lab Chip*, 2023, **23**, 1258–1278, DOI: **10.1039/D2LC00814A**.
6 Y. Hou, S. Chen, Y. Zheng, X. Zheng and J.-M. Lin, *TrAC, Trends Anal. Chem.*, 2023, **158**, 116897, DOI: **10.1016/j.trac.2022.116897**.
7 A. A. Kojabad, M. Farzanehpour, H. E. G. Galeh, R. Dorostkar, A. Jafarpour, M. Bolandian and M. M. Nodooshan, *J. Med. Virol.*, 2021, **93**, 4182–4197, DOI: **10.1002/jmv.26846**.
8 E. A. Ottesen, J. W. Hong, S. R. Quake and J. R. Leadbetter, *Science*, 2006, **314**, 1464–1467, DOI: **10.1126/science.1131370**.
9 F. Shen, W. Du, J. E. Kreutz, A. Fok and R. F. Ismagilov, *Lab Chip*, 2010, **10**, 2666–2672, DOI: **10.1039/C004521G**.
10 Y. Yu, Z. Yu, X. Pan, L. Xu, R. Guo, X. Qiana and F. Shen, *Analyst*, 2022, **147**, 625–633, DOI: **10.1039/D1AN01916C**.

11 Y. Luo, Q. Hu, Y. Yu, W. Lyu and F. Shen, *Anal. Chim. Acta*, 2024, **1304**, 342541, DOI: **10.1016/j.aca.2024.342541**.
12 T. Morrison, J. Hurley, J. Garcia, K. Yoder, A. Katz, D. Roberts, J. Cho, T. Kanigan, S. E. Ilyin, D. Horowitz, J. M. Dixon and C. J. H. Brenan, *Nucleic Acids Res.*, 2006, **34**, e123, DOI: **10.1093/nar/gkl639**.
13 J. Li, Y. Qiu, Z. Zhang, C. Li, S. Li, W. Zhang, Z. Guo, J. Yaoad and L. Zhou, *Analyst*, 2020, **145**, 3116–3124, DOI: **10.1039/D0AN00220H**.
14 C. D. Ahrberg, J. M. Lee and B. G. Chung, *BioChip J.*, 2019, **13**, 269–276, DOI: **10.1007/s13206-019-3302-8**.
15 Y. Men, Y. Fu, Z. Chen, P. A. Sims, W. J. Greenleaf and Y. Huang, *Anal. Chem.*, 2012, **84**, 4262–4266, DOI: **10.1021/ac300761n**.
16 K. A. Heyries, C. Tropini, M. VanInsberghe, C. Doolin, O. I. Petriv, A. Singhal, K. Leung, C. B. Hughesman and C. L. Hansen, *Nat. Methods*, 2011, **8**, 649–651, DOI: **10.1038/nmeth.1640**.
17 M. E. Dueck, R. Lin, A. Zayac, S. Gallagher, A. K. Chao, L. Jiang, S. S. Datwani, P. Hung and E. Stieglitz, *Sci. Rep.*, 2019, **9**, 19606, DOI: **10.1038/s41598-019-55872-7**.
18 A. M. Thompson, A. Gansen, A. L. Paguirigan, J. E. Kreutz, J. P. Radich and D. T. Chiu, *Anal. Chem.*, 2014, **86**, 12308–12314, DOI: **10.1021/ac5035924**.
19 J. Wang, J. E. Kreutz, A. M. Thompson, Y. Qin, A. M. Sheen, J. Wang, L. Wu, S.n. Xu, M. Chang, D. N. Raugi, R. A. Smith, G. S. Gottlieb and D. T. Chiu, *Lab Chip*, 2018, **18**, 3501–3506, DOI: **10.1039/C8LC00956B**.
20 Q. Zhu, L. Qiu, B. Yu, Y. Xu, Y. Gao, T. Pan, Q. Tian, Q. Song, W. Jin, Q. Jin and Y. Mu, *Lab Chip*, 2014, **14**, 1176–1185, DOI: **10.1039/C3LC51327K**.
21 Q. Zhu, Y.n. Xu, L. Qiu, C. Ma, B. Yu, Q. Song, W. Jin, Q. Jin, J. Liu and Y. Mu, *Lab Chip*, 2017, **17**, 1655–1665, DOI: **10.1039/C7LC00267J**.
22 H. Si, G. Xu, F. Jing, P. Sun, D. Zhao and D. Wu, *Sens. Actuators, B*, 2020, **318**, 128197, DOI: **10.1016/j.snb.2020.128197**.
23 X. Cui, L. Wu, Y. Wu, J. Zhang, Q. Zhao, F. Jing, L. Yi and G. Li, *Anal. Chim. Acta*, 2020, **1107**, 127–134, DOI: **10.1016/j.aca.2020.02.010**.
24 G. Xu, H. Si, F. Jing, P. Sun, D. Zhao and D. Wu, *Micromachines*, 2020, **11**, 1025, DOI: **10.3390/mi11121025**.
25 K. Hosokawa and H. Ohmori, *Anal. Sci.*, 2023, **39**, 2067–2074, DOI: **10.1007/s44211-023-00425-2**.
26 H. Yuan, Y. Chao and H. C. Shum, *Small*, 2020, **16**, 1904469, DOI: **10.1002/smll.201904469**.
27 H. Zhang, Y. Xu, Z. Fohlerova, H. Chang, C. Iliescu and P. Neuzil, *TrAC, Trends Anal. Chem.*, 2019, **113**, 44–53, DOI: **10.1016/j.trac.2019.01.015**.
28 Y. Zeng, C. Wu and Y. He, *Curr. Infect. Dis. Rep.*, 2022, **24**, 205–215, DOI: **10.1007/s11908-022-00790-5**.
29 D. Das, C.-W. Lin and H.-S. Chuang, *Biosensors*, 2022, **12**, 1068, DOI: **10.3390/bios12121068**.
30 T. Notomi, H. Okayama, H. Masubuchi, T. Yonekawa, K. Watanabe, N. Amino and T. Hase, *Nucleic Acids Res.*, 2000, **28**, e63, DOI: **10.1093/nar/28.12.e63**.
31 K. Nagamine, T. Hase and T. Notomi, *Mol. Cell. Probes*, 2002, **16**, 223–229, DOI: **10.1006/mcpr.2002.0415**.
32 L. Becherer, N. Borst, M. Bakheit, S. Frischmann, R. Zengerle and F. von Stetten, *Anal. Methods*, 2020, **12**, 717–746, DOI: **10.1039/C9AY02246E**.
33 T. D. Rane, L. Chen, H. C. Zec and T.-H. Wang, *Lab Chip*, 2015, **15**, 776–782, DOI: **10.1039/C4LC01158A**.
34 Y.-D. Ma, K. Luo, W.-H. Chang and G.-B. Lee, *Lab Chip*, 2018, **18**, 296–303, DOI: **10.1039/C7LC01004D**.
35 H. Yuan, Y. Chao, S. Li, M. Y. H. Tang, Y. Huang, Y. Che, A. S. T. Wong, T. Zhang and H. C. Shum, *Anal. Chem.*, 2018, **90**, 13173–13177, DOI: **10.1021/acs.analchem.8b03673**.
36 M. Azizi, M. Zaferani and S. H. Cheong, *ACS Sens.*, 2019, **4**, 841–848, DOI: **10.1021/acssensors.8b01206**.
37 Y. Wang, X. Zhou, Z. Yang, T. Xu, H. Fu, C.-C. Fong, J. Sun, Y. R. Chin, L. Zhang, X. Guan and M. Yang, *Biosens. Bioelectron.*, 2024, **246**, 115831, DOI: **10.1016/j.bios.2023.115831**.
38 B. Sun, F. Shen, S. E. McCalla, J. E. Kreutz, M. A. Karymov and R. F. Ismagilov, *Anal. Chem.*, 2013, **85**, 1540–1546, DOI: **10.1021/ac3037206**.
39 J. Rodriguez-Manzano, M. A. Karymov, S. Begolo, D. A. Selck, D. V. Zhukov, E. Jue and R. F. Ismagilov, *ACS Nano*, 2016, **10**, 3102–3113, DOI: **10.1021/acsnano.5b07338**.
40 M. Yu, X. Chen, H. Qu, L. Ma, L. Xu, W. Lv, H. Wang, R. F. Ismagilov, M. Li and F. Shen, *Anal. Chem.*, 2019, **91**, 8751–8755, DOI: **10.1021/acs.analchem.9b01270**.
41 W. Lyu, J. Zhang, Y. Yu, L. Xu and F. Shen, *Lab Chip*, 2021, **21**, 3086–3093, DOI: **10.1039/D1LC00361E**.
42 A. Gansen, A. M. Herrick, I. K. Dimov, L. P. Lee and D. T. Chiu, *Lab Chip*, 2012, **12**, 2247–2254, DOI: **10.1039/C2LC21247A**.
43 J. E. Kreutz, J. Wang, A. M. Sheen, A. M. Thompson, J. P. Staheli, M. R. Dyen, Q. Feng and D. T. Chiu, *Lab Chip*, 2019, **19**, 1035–1040, DOI: **10.1039/C8LC01223G**.
44 J. Wang, J. P. Staheli, A. Wu, J. E. Kreutz, Q. Hu, J. Wang, T. Schneider, B. S. Fujimoto, Y. Qin, G. S. Yen, B. Weng, K. Shibley, H. Haynes, R. L. Winer, Q. Feng and D. T. Chiu, *Anal. Chem.*, 2021, **93**, 3266–3272, DOI: **10.1021/acs.analchem.0c04973**.
45 Q. Zhu, Y. Gao, B. Yu, H. Ren, L. Qiu, S. Han, W. Jin, Q. Jin and Y. Mu, *Lab Chip*, 2012, **12**, 4755–4763, DOI: **10.1039/C2LC40774D**.
46 X. Zhang, X. Li, Q. Liu, S. Ke, Y. Ji, S. Liu and G. Sui, *Sens. Actuators, B*, 2019, **278**, 8–14, DOI: **10.1016/j.snb.2018.09.020**.
47 Y. Xia, S. Yan, X. Zhang, P. Ma, W. Du, X. Feng and B.-F. Liu, *Anal. Chem.*, 2017, **89**, 3716–3723, DOI: **10.1021/acs.analchem.7b00031**.
48 T. Kasputis, P.-C. Yeh, L. Liu, J. Marano, J. Weger-Lucarelli, K. Du, L. Lin and J. Chen, *Lab Chip*, 2024, **24**, 3490–3497, DOI: **10.1039/D4LC00265B**.
49 Y.-D. Ma, W.-H. Chang, K. Luo, C.-H. Wang, S.-Y. Liu, W.-H. Yen and G.-B. Lee, *Biosens. Bioelectron.*, 2018, **99**, 547–554, DOI: **10.1016/j.bios.2017.08.026**.
50 B. Lin, Z. Guo, Z. Geng, S. Jakaratanopas, B. Han and P. Liu, *Lab Chip*, 2020, **20**, 2981–2989, DOI: **10.1039/D0LC00348D**.

51 D. Natsuhara, K. Takishita, K. Tanaka, A. Kage, R. Suzuki, Y. Mizukami, N. Saka, M. Nagai and T. Shibata, *Micromachines*, 2020, **11**, 540, DOI: **10.3390/mi11060540**.

52 S. Misawa, D. Natsuhara, Y. Kiba, T. Yamamuro, R. Suzuki, T. Shibata and M. Kitamura, *Forensic Toxicol.*, 2021, **39**, 259–265, DOI: **10.1007/s11419-020-00557-4**.

53 D. Natsuhara, R. Saito, H. Aonuma, T. Sakurai, S. Okamoto, M. Nagai, H. Kanuka and T. Shibata, *Lab Chip*, 2021, **21**, 4779–4790, DOI: **10.1039/D1LC00829C**.

54 D. Natsuhara, S. Misawa, R. Saito, K. Shirai, S. Okamoto, M. Nagai, M. Kitamura and T. Shibata, *Sci. Rep.*, 2022, **12**, 12852, DOI: **10.1038/s41598-022-16945-2**.

55 D. Natsuhara, A. Miyajima, T. Bussho, S. Okamoto, M. Nagai, M. Ihira and T. Shibata, *Analyst*, 2024, **149**, 3335–3345, DOI: **10.1039/D4AN00215F**.

56 D. Natsuhara, Y. Kiba, R. Saito, S. Okamoto, M. Nagai, Y. Yamauchi, M. Kitamura and T. Shibata, *RSC Adv.*, 2024, **14**, 22606–22617, DOI: **10.1039/D4RA04055D**.

57 A. Miyajima, F. Nishimura, D. Natsuhara, Y. Kiba, S. Okamoto, M. Nagai, T. Yamamuro, M. Kitamura and T. Shibata, *Lab Chip*, 2025, **25**, 3242–3253, DOI: **10.1039/D5LC00356C**.

58 H. Ou, Y. Wang, J. Gao, J. Bai, Q. Zhang, L. Shi, X. Wang and C. Wang, *Ann. Palliat. Med.*, 2021, **10**, 6850–6858, DOI: **10.21037/apm-21-1387**.

59 M. Kitamura, M. Aragane, K. Nakamura, K. Watanabe and Y. Sasaki, *Biol. Pharm. Bull.*, 2016, **39**, 1144–1149, DOI: **10.1248/bpb.b16-00090**.

60 M. K. Nwe, N. Jangpromma and L. Taemaitree, *Sci. Rep.*, 2024, **14**, 59164, DOI: **10.1038/s41598-024-55241-z**.

61 T. L. Dangerfield, I. Paik, S. Bhadra, K. A. Johnson and A. D. Ellington, *Nucleic Acids Res.*, 2023, **51**, 488–499, DOI: **10.1093/nar/gkac1221**.

62 G. D. Weiblen, J. P. Wenger, K. J. Craft, M. A. ElSohly, Z. Mehmedic, E. L. Treiber and M. D. Marks, *New Phytol.*, 2015, **208**, 1241–1250, DOI: **10.1111/nph.13562**.